

# Investigating cocoa butter crystallization using rheology and Raman spectroscopy

## Authors

Nathan C. Crawford and Mohammed Ibrahim Thermo Fisher Scientific  
Madison WI, USA

## Keywords

Cocoa butter, crystallization, Raman spectroscopy, rheology, RheoRaman, *in situ*, storage modulus  $G'$ , loss modulus  $G''$

## Thermo Scientific solutions

- HAAKE MARS 60 Rheometer
- DXR3 Flex Raman Spectrometer
- RheoRaman Module for Haake MARS Rheometers
- OMNIC software for dispersive Raman software

## Application benefits

Simultaneous rheology and Raman spectroscopy (RheoRaman) measurements were used to examine the isothermal crystallization of cocoa butter (CB). The results indicate that CB crystallized by first hardening into an amorphous solid. The amorphous–solid then underwent a morphological transition to form a crystalline solid. Without coupling these two separate analytical techniques, the observed amorphous–solid to crystalline–solid transformation would have been left undetected. Alone, each technique suggests a single-stage process; however, only when the two techniques are coupled is the multi-phase crystallization process revealed, further exemplifying the unique analytical capability unleashed by hyphenating rheology with *in situ* Raman spectroscopy.

## Introduction

CB is an edible vegetable fat extracted from the cocoa bean. CB is commonly used in home and personal care products (such as ointments and lotions). CB is also a vital ingredient in chocolate, forming the continuous phase within chocolate confections, and is responsible for the chocolate's texture, snap, gloss, melting behavior, and resistance to fat bloom. These physical characteristics are a direct result of CB's triacylglycerol (TAG) composition and overall crystalline structure.

In general, TAG molecules assume a tuning fork configuration and these TAG forks assemble to form crystal lattice structures. During crystallization, the TAG molecules slow down as the CB oil cools and the TAGs come to rest in contact with one another, forming what are known as subcrystalline cells.<sup>1</sup> Once the subcrystalline cells are formed, they are thermodynamically driven to aggregate into larger and more stable crystalline structures.<sup>2</sup> The self-assembly of subcrystalline-cell structures and their further aggregation is governed by a balance of intra- and inter-molecular interactions. Depending on the molecular level packing and orientation, CB can form different types of crystal lattice structures (or polymorphs), where some crystal structures are more desirable than others. Overall, CB crystallization is a highly complex, multistage process. Understanding the isothermal crystallization behavior of CB is vital for improving chocolate manufacturing processes and maintaining product quality.

In this application note, rheology coupled with in situ Raman spectroscopy was used to examine the isothermal crystallization of CB. Raman spectroscopy is a highly sensitive, relatively fast, and nondestructive technique that can probe the molecular structure and conformation in both liquid and solid TAG assemblies, as well as intra- and inter-TAG interactions. With simultaneous Raman spectra and rheological data, molecular-level interactions and conformational shifts during the isothermal crystallization of CB were directly correlated with the changes in bulk viscoelastic properties, providing unique insight into the multifaceted crystallization behavior of CB.

## Materials and methods

### Materials

Commercially available, organic CB (*Theobroma cacao*) was acquired from Inesscents Aromatic Botanicals (Ashland, OR, USA).

### Raman spectroscopy

Raman spectroscopy measurements were performed using a Thermo Scientific™ DXR3 Flex Raman Spectrometer. A 532 nm laser was used with 10 mW laser power at the sample. The spectral range was 50–3500  $\text{cm}^{-1}$ . The spectra were collected using a two-second exposure time and four sample exposures. Data acquisition and processing were controlled by Thermo Scientific OMNIC™ Software for Dispersive Raman. For the data presented here, sequential Raman spectra (in parallel with the rheological measurements) were collected over a predetermined time window using the time series collection function of OMNIC Series Software.

### Rheology

Rheological measurements were performed using a Thermo Scientific HAAKE™ MARS 60 Rheometer equipped with a serrated 35 mm diameter plate rotor at a gap height of 1 mm. The serrated plate was used to prevent slip at the sample-rotor interface.

All measurements were conducted in the oscillatory mode, with a frequency of 1 Hz and a constant strain of 0.1%. CB samples were loaded onto the rheometer at 60°C and allowed to equilibrate for 10 minutes to erase any crystal structures and/or shear history from sample loading. After the equilibrium step, the temperature was rapidly decreased from 60°C to 22°C at a rate of 10°C/min. The temperature was then held constant at 22°C for 120 minutes, collecting data every 10 seconds.

### RheoRaman coupling

The Thermo Scientific HAAKE™ MARS RheoRaman System consists of the DXR3 Flex Raman Spectrometer and the HAAKE MARS 60 Rheometer coupled together using the HAAKE RheoRaman module (Figure 1). The DXR3 Flex Raman Spectrometer was free-space coupled to the rheometer with an optical train, using a series of mirrors to direct the incident laser into the RheoRaman module (Figure 1). Within the module, a mirror directed the laser beam into a 20x objective, and the laser light was focused into the sample (perpendicularly to the flow or vorticity plane). Backscattered Raman light was collected using the same 20x objective and guided back to the spectrometer using the same optical train as the incident laser, eventually reaching the spectrograph inside the spectrometer (Figure 1).

The sample was positioned between a sandblasted glass bottom plate and the serrated 35 mm plate rotor, using textured plates to avoid slip at the sample-plate interfaces. An electrical heating element within the RheoRaman module provided temperature control from below the sample, while an active electrical hood was used to provide temperature control from above, eliminating the potential for a temperature gradient within the sample. Cooling of the sample was supplied from a temperature-controlled water bath circulator.

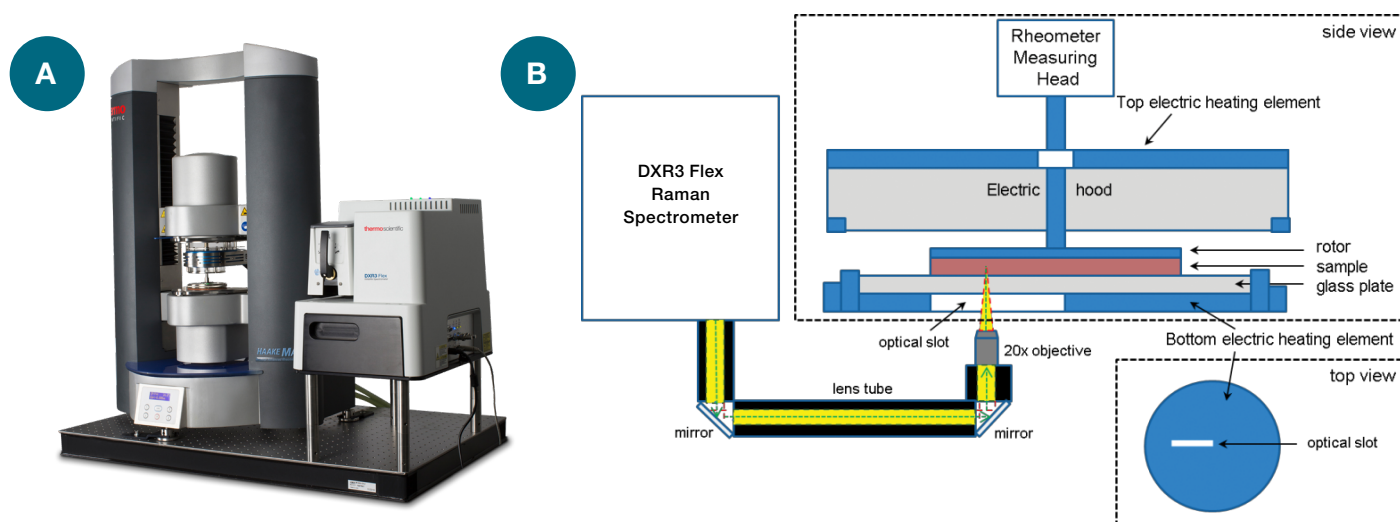


Figure 1. (a) RheoRaman module for the The Thermo Scientific HAAKE™ MARS RheoRaman System. (b) Schematic diagram of the MARS RheoRaman System (showing side and top views of the rheometer sample stage). The DXR3 Flex Raman Spectrometer is free-space coupled to the MARS rheometer using lens tubes and mirrors that direct light into a 20x objective. The objective focuses the incoming laser (green dashed line) and collects the back-scattered Raman light (yellow) coming out of the sample sitting atop the rheometer stage.

## Results and discussion

### Raman spectroscopy: CB crystallization

Raman spectra for the liquid phase CB melt and the crystalline solid CB in the 500–3000  $\text{cm}^{-1}$  range are shown in Figure 2. Prominent Raman features were observed in both the C–H stretching region (2700–3050  $\text{cm}^{-1}$ ) and the fingerprint region (1000–1800  $\text{cm}^{-1}$ ). More specifically, the lower Raman shift features include: the carbonyl (C=O).

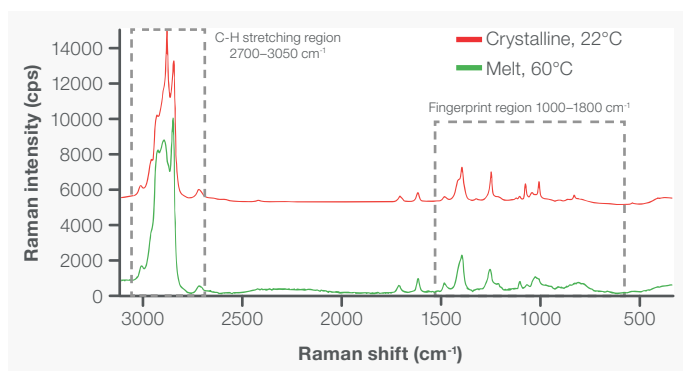


Figure 2. The full Raman spectra of melted and crystalline CB.

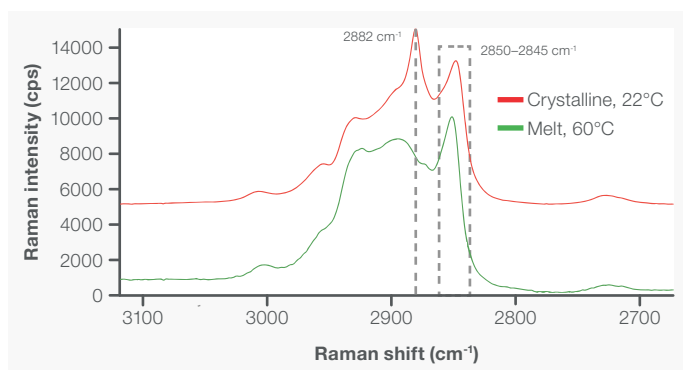


Figure 3. Raman spectra of the C–H stretching region (2700–3050  $\text{cm}^{-1}$ ) for melted and crystalline CB.

Although less intense than the C–H stretching region, approximately eight unique spectral features were identified in the fingerprint region (1000–1800  $\text{cm}^{-1}$ ; Figure 4). When comparing the CB melt state to the crystalline phase, the most significant changes were observed in the C–C stretching region (1000–1200  $\text{cm}^{-1}$ ), stretching region (1700–1800  $\text{cm}^{-1}$ ), the olefinic (C=C) band at  $\sim 1655$   $\text{cm}^{-1}$ , the CH<sub>3</sub> and CH<sub>2</sub> deformations ( $\sim 1460$  and  $1440$   $\text{cm}^{-1}$ , respectively), the CH<sub>2</sub> twisting region (1250–1300  $\text{cm}^{-1}$ ), and the C–C stretching region (1000–1200  $\text{cm}^{-1}$ ).

The C–H stretching regions for the melted and solidified CB specimens are highlighted in Figure 3. Two strong peaks were observed at  $\sim 2850$   $\text{cm}^{-1}$  and  $2882$   $\text{cm}^{-1}$ , which are attributed to symmetric and asymmetric CH<sub>2</sub> stretching, respectively.<sup>2</sup> The symmetric vibrational modes at  $2850$   $\text{cm}^{-1}$  were dominant in the liquid (melt) phase, while the asymmetric vibrations at  $2882$   $\text{cm}^{-1}$  were dominant in the solid phase.

Thus, the  $2850$   $\text{cm}^{-1}$  and  $2882$   $\text{cm}^{-1}$  bands are strong indicators of amorphous and crystalline content, respectively.<sup>3</sup> Subsequently, the  $I_{2882}/I_{2850}$  peak intensity ratio was used to dynamically track crystal formation during the *in situ* RheoRaman measurements.

Two well-defined features emerged at  $1130$   $\text{cm}^{-1}$  and  $1063$   $\text{cm}^{-1}$  during the solidification process, which originated from the symmetric and asymmetric C–C stretching, respectively.<sup>4,5</sup> In the melt phase, all C–C stretching bands were relatively weak and broad due to the disordering effects of methyl gauche conformations.

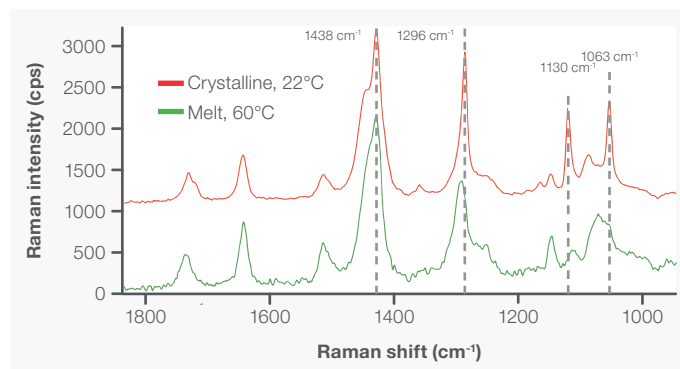


Figure 4. The 1000–1800  $\text{cm}^{-1}$  Raman spectral range for melted and crystalline CB.

However, as the CB solidified, the backbone methyl groups were ordered into the trans-conformation, signified by the emergence of the peak at  $1130$   $\text{cm}^{-1}$ . Therefore, in addition to the  $I_{2882}/I_{2850}$  peak intensity ratio, the  $I_{1130}/I_{12850}$  spectral marker was also used to track the crystalline-phase transition within CB via *in situ* RheoRaman measurements.

### Simultaneous rheology and Raman spectroscopy (RheoRaman)

The melt-to-solid phase transition of CB was probed rheologically using small amplitude oscillatory shear measurements (Figure 5a), where the storage modulus  $G'$  and loss modulus  $G''$  were measured as a function of time at the isothermal temperature of  $22^\circ\text{C}$ .  $G'$  and  $G''$  are measures of a material's elastic and viscous behavior, respectively. A liquid-like material will be more viscous than elastic (i.e., viscously dominated), and as a result,  $G''$  will be greater than  $G'$ . Conversely, a solid-like material will display more elastic than viscous behavior (i.e., elastically dominated), where  $G'$  will be greater than  $G''$ . The overall magnitudes of  $G'$  and  $G''$ , as well as their relative difference in magnitude, often reported as the ratio of  $G''/G'$ , determines the general viscoelasticity and overall resistance to deformation for a given material.

The ratio of  $G''/G'$  (plotted on the right y-axis of Figure 5a) is commonly used to track viscoelasticity of a material: where  $\delta$

$$\frac{G''}{G'} = \tan(\delta),$$

is the phase angle defined as the shift or lag between the input strain and resultant stress sine waves (or vice versa) during an oscillatory shear measurement. The term “ $\tan(\delta)$ ” is often referred to as the loss or damping factor. Values of  $\tan(\delta)$  less than unity indicate elastically dominant (solid-like) behavior, while values greater than unity indicate viscously dominant (liquid-like) behavior.

Unlike the individual moduli,  $\tan(\delta)$  can be used to quantify overall brittleness of a material and is commonly used to assess glass transition behavior. In general, as  $\tan(\delta)$  becomes smaller, the more  $G'$  deviates from  $G''$ , and the more brittle (or glass-like) the material becomes.

During the initial portion of the isothermal hold at 22°C from 0 to 5 min (immediately following the rapid decrease in temperature from 60°C to 22°C), both  $G'$  and  $G''$  increased as the CB transformed from a melted liquid to a soft semisolid (Figure 5a). This initial increase in modulus is most likely due to a delay between the set temperature and the internal temperature of the loaded sample. Once the sample had reached thermal equilibrium and was at the isothermal set point of 22°C, the moduli were relatively stable from 10 to 25 minutes. From 25 to 50 minutes, however, both  $G'$  and  $G''$  begin to gradually increase and then from 50 to 80 minutes, the moduli rapidly increased, where  $G'$  and  $G''$  increased by approximately 5 and 4 orders of magnitude, respectively. The exponential increase in the moduli indicates a solidification process, where the CB transformed from a pliable semisolid to a more robust, hardened solid. At 80 minutes and beyond, growth in the elastic modulus slowed and eventually plateaued, showing no further significant change past 100 minutes. The viscous modulus, however, reached a slight plateau from 80 to 100 minutes and then proceeded to gradually decrease from 100 minutes and beyond.

During the increase in  $G'$  and  $G''$ , a rapid decrease in the loss factor  $\tan(\delta)$  was observed from ~65 minutes and beyond (Figure 5a, right y-axis). The decrease in the loss factor indicates a deviation in overall magnitude between  $G'$  and  $G''$ . As the CB hardened, the increase in  $G'$  exceeded the increase in  $G''$ , triggering the decrease in  $\tan(\delta)$ . At the end of the 120 minutes isothermal study,  $G'$  was more than a full order of magnitude greater than  $G''$  and the loss factor was approaching 0.01, indicating the CB had transitioned into a brittle glass-like solid.

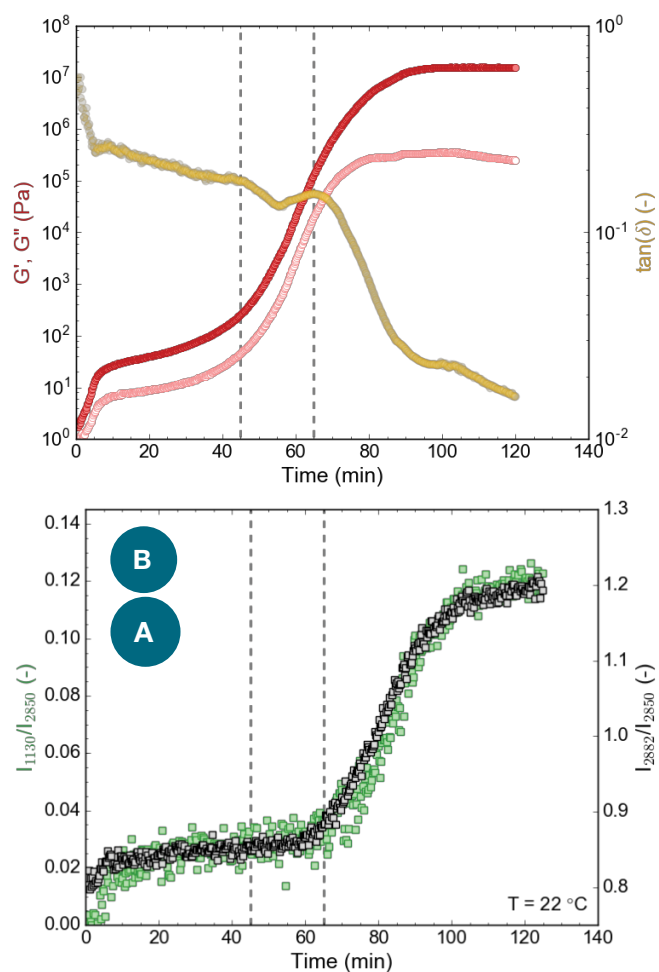


Figure 5. (a) Rheology:  $G'$  and  $G''$  (filled and open circles, respectively; plotted on the left y-axis) and  $\tan(\delta)$  (plotted on the right y-axis) and (b) Raman: the  $I_{1130}/I_{2850}$  (left y-axis, green) and  $I_{2882}/I_{2850}$  (right y-axis, black) peak intensity ratios for CB during isothermal crystallization at 22°C. The vertical dashed line at 45 minutes indicates the increase of  $G'$  and  $G''$ , while the dashed line at 65 minutes indicates the decrease in  $\tan(\delta)$  and increase in the Raman ratios.

The observed rheological behavior was further confirmed using simultaneous Raman spectroscopy (Figure 5b). Initially, both the  $I_{1130}/I_{2850}$  and  $I_{2882}/I_{2850}$  peak intensity ratios remained unchanged during the first ~65 minutes of the isothermal study. Then a sharp increase of the  $I_{1130}/I_{2850}$  and  $I_{2882}/I_{2850}$  ratios began at ~65 minutes, indicating the formation of crystal structures within the CB. As the CB further crystallized, both spectral markers continued to increase from 65 to 100 minutes. Beyond 100 minutes, the growth in both Raman features had subsided and the peak intensity ratios began to stabilize.

Overall, the rate of increase in the 1130 and 2882  $\text{cm}^{-1}$  spectral ratios was similar to the rate of change for both  $G'$  and  $G''$  (i.e., they increased with similar slopes). However, there was a noticeable 15- to 20-minute lag between the observed increase in  $G'$  and  $G''$  and the rise of the Raman intensity ratios. The sharp upturn in  $G'$  and  $G''$  indicates an increased resistance to deformation (i.e., a bulk hardening of the CB), signaling the start of the solidification process. The Raman spectral markers, on the other hand, are indicators of crystal formation. Thus, the time delay between the rheology and Raman profiles suggests that CB first hardens into an amorphous solid, followed by a transformation from an amorphous to a crystalline solid. This morphological transformation was signified by the subsequent increase in the Raman band intensities associated with crystal CB structures (the 1130 and 2882  $\text{cm}^{-1}$  peaks). The temporal separation of the rheological and Raman spectral profiles indicates a clear distinction between bulk hardening of the CB and the formation of crystalline domains.

Interestingly, the increase in the Raman spectral features ( $I_{1130}/I_{2850}$  and  $I_{2882}/I_{2850}$ ) directly correlated with the observed reduction in  $\tan(\delta)$  (Figure 5). The loss factor is an indication of material brittleness and crystalline structures are commonly known to be brittle. Thus, it is reasonable that the formation of crystal domains at the molecular level (as indicated by Raman) coincides with the overall brittleness of the CB. As a result, the loss factor may be a more revealing indicator of bulk CB crystallization than  $G'$  and  $G''$  alone.

## Conclusions

Simultaneous rheology and Raman spectroscopy measurements were used to examine the isothermal crystallization of CB. This multimodal analytical technique allowed the bulk mechanical properties of CB ( $G'$ ,  $G''$ , and  $\tan(\delta)$ ) to be directly correlated with conformational changes at the molecular level ( $\nu_{\text{as}}(\text{CH}_2)$  mode at 2882  $\text{cm}^{-1}$  and the  $\nu_{\text{s}}(\text{C-C})$  mode at 1130  $\text{cm}^{-1}$ ) in real time. After rapid cooling (10°C /minutes) and at an isothermal temperature of 22°C, there was a noticeable time lag between the rheological response ( $G'$  and  $G''$ ) and the Raman spectral profiles. The observed time delay indicates that CB crystallized by first hardening into an amorphous solid, manifested by a sharp increase in  $G'$  and  $G''$ , while the Raman features remained unchanged.

The amorphous solid then underwent a morphological transition to form a crystalline solid, signified by the increase in Raman features associated with crystal CB structures (1130 and 2882  $\text{cm}^{-1}$ ). Without coupling these two separate analytical techniques, the observed amorphous–solid to crystalline–solid transformation would have been left undetected. Alone, each technique suggests a single stage process, however, only when the two techniques are coupled is the multiphase crystallization process revealed, further exemplifying the unique analytical capability unleashed by hyphenating rheology with *in situ* Raman spectroscopy. While this work focuses on the isothermal crystallization of CB, the underlying principles applied here should be applicable for a wide range of material processes including gelation, polymerization, curing behavior, as well as other shear-induced phenomena.

## References

1. K. Sato, *Crystallization of Lipids: Fundamentals and Applications in Food, Cosmetics, and Pharmaceuticals*. Hoboken, NJ: John Wiley & Sons, 2018.
2. S. Bresson, D. Rousseau, S. Ghosh, M. El Marssi, and V. Faivre, Raman spectroscopy of the polymorphic forms and liquid state of cocoa butter, *Eur. J. Lipid Sci. Technol.* 113, 992–1004, 2011.
3. R. G. Snyder, H. L. Strauss, and C. A. Elliger, C–H stretching modes and the structure of n-alkyl chains. 1. Long, disordered chains, *J. Phys. Chem.* 86, 5145–5150, 1982.
4. R. J. Meier, Studying the length of trans conformational sequences in polyethylene using Raman spectroscopy: A computational study, *Polymer*. 43, 517–522, 2002.
5. M. Zheng and M. Du, Phase behavior, conformations, thermodynamic properties, and molecular motion of multicomponent paraffin waxes: A Raman spectroscopy study. *Vib. Spectrosc.* 40, 219–224, 2006.

Learn more at [thermofisher.com/Raman](https://thermofisher.com/Raman)  
or [thermofisher.com/rheology](https://thermofisher.com/rheology)

thermo scientific

For research use only. Not for use in diagnostic procedures. For current certifications, visit [thermofisher.com/certifications](https://thermofisher.com/certifications)

© 2024 Thermo Fisher Scientific Inc. All rights reserved. All trademarks are the property of Thermo Fisher Scientific and its subsidiaries unless otherwise specified. V-295 & AN53002\_E 04/24M